

# Impact of Wingsail Integration on Seakeeping Performance and Stability of a Fishing Vessel

Hegel Desta Zalayetha<sup>1</sup>, Mohammad Ridwan Utina<sup>2</sup>, Dian Purnamasari<sup>3</sup>, Endah Suwarni<sup>4</sup>, Wiwin Sulistyawati<sup>5</sup>

(Received: 19 March 2026 / Revised: 27 March 2026 / Accepted: 30 March 2026 / Available Online: 30 March 2026)

**Abstract**— Wind-assisted propulsion systems (WASP) have emerged as a promising approach to reduce fuel consumption and emissions in maritime operations; however, their application on small-scale fishing vessels remains limited. This study aims to evaluate the effect of rigid wingsail integration on the seakeeping performance and intact stability of a 33.5 m tuna longliner. The analysis was conducted using numerical simulations, where seakeeping performance was assessed using Maxsurf Motions and stability characteristics were evaluated using Maxsurf Stability under various operational conditions. The results indicate that adding the wingsail does not produce significant changes in vessel motion responses or stability parameters. All evaluated conditions satisfy the applicable seakeeping and intact stability criteria. These findings suggest that wingsail integration is technically feasible and can be safely applied to fishing vessels without compromising operational performance.

**Keywords**— WASP, Fishing Vessel, Seakeeping, Stability, Wingsail

\*Corresponding Author: 2210313023@mahasiswa.upnvj.ac.id

## I. INTRODUCTION

Indonesia, as the world's largest archipelagic country, relies heavily on the marine and fisheries sectors to support national food security and coastal economies. Fishing vessels play a crucial role in harvesting marine resources, particularly in small- to medium-scale fisheries. However, their operations are highly dependent on fossil fuels, leading to higher operational costs and increased vulnerability to fuel price fluctuations [1].

Recently, wind-assisted propulsion systems (WASP) have gained attention as a way to improve energy efficiency and reduce greenhouse gas emissions in maritime transportation. Several WASP technologies, wingsails, Flettner rotors, kite systems, and wind turbines have been investigated and can reduce fuel use [2], [3]. Of these, rigid wingsails show promise thanks to high aerodynamic efficiency and structural reliability [4].

Previous studies have predominantly focused on the aerodynamic performance and energy-saving potential of wingsail systems. Symmetric airfoil profiles, such as NACA 0015, are widely adopted due to their balanced lift characteristics [5], while wingsail configuration and arrangement significantly influence aerodynamic

efficiency [6]. Despite these advancements, most studies emphasise propulsion benefits and provide limited discussion on the hydrodynamic implications of wingsail installation.

From a hydrodynamic perspective, the addition of a wingsail alters the mass distribution, centre of gravity, and wind-exposed area, which may influence vessel motion responses and stability characteristics [8],[19]. Earlier studies have shown that sail-assisted systems can affect roll motion, particularly near resonance, while their influence on pitch motion remains relatively small [7]. Furthermore, additional wind-induced heeling moments require careful evaluation of the balance between external forces and the vessel's restoring capability [8].

However, existing research has largely focused on large commercial vessels with relatively stable loading conditions. In contrast, fishing vessels are highly sensitive to loading conditions and motion response [9], while improvements in seakeeping performance have been linked to parameters such as radius of gyration [10]. However, studies specifically addressing WASP applications on fishing vessels remain limited [11].

Therefore, the main problem addressed in this study is the lack of a comprehensive understanding of how wingsail integration affects both seakeeping performance and intact stability of small-scale fishing vessels. The uncertainty regarding these effects raises concerns about operational safety and limits the practical adoption of WASP technology in the fisheries sector.

To fill this gap, the study evaluates how rigid wingsails affect seakeeping and stability of a 33.5 m tuna longliner. Numerical simulation uses Maxsurf Motions for seakeeping, and Maxsurf Stability for intact stability, under typical operating conditions.

This research provides three main novelties. First, it integrates seakeeping and intact-stability assessment for a fishing vessel with wingsails, a combination that has rarely been done before. Second, it uses realistic operating scenarios based on actual field data from

---

Hegel Desta Zalayetha, Department of Naval Engineering, Universitas Pembangunan Nasional Veteran Jakarta, Jakarta 12450, Indonesia, E-mail: 2210313023@mahasiswa.upnvj.ac.id

Mohammad Ridwan Utina, Pusat Riset Teknologi Hidrodinamika, Badan Riset dan Inovasi Nasional, Surabaya 60112, Indonesia, E-mail: muha009@brin.go.id

Dian Purnamasari, Pusat Riset Teknologi Hidrodinamika, National Research and Innovation Agency (BRIN), Surabaya, E-mail: dian010@brin.go.id

Endah Suwarni, Pusat Riset Teknologi Hidrodinamika, National Research and Innovation Agency (BRIN), Surabaya, E-mail: nda032@brin.go.id

Wiwin Sulistyawati, Department of Naval Engineering, Universitas Pembangunan Nasional Veteran Jakarta, Jakarta 12450, Indonesia, E-mail: wiwin.sulistyawati@upnvj.ac.id

Indonesian waters. Third, it evaluates vessel performance using both NATO STANAG 4154 seakeeping criteria and the IMO Intact Stability Code 2008 [18], [20]. These contributions help assess the safety and technical feasibility of wingsails for small fishing vessels.

## II. Method

### A. Vessel and Sail configuration

#### a) Fishing Vessel

A fishing vessel integrated with a rigid wind-assisted propulsion system (WASP) is used as the case study. The hull geometry was developed in AutoCAD using the principal dimensions of a representative Indonesian fishing vessel. The principal vessel data were obtained through field surveys conducted in the waters of Benoa, Bali, including direct observations and interviews with operating fishing fleets and representatives of the Indonesian Tuna Longline Association (ATLI).

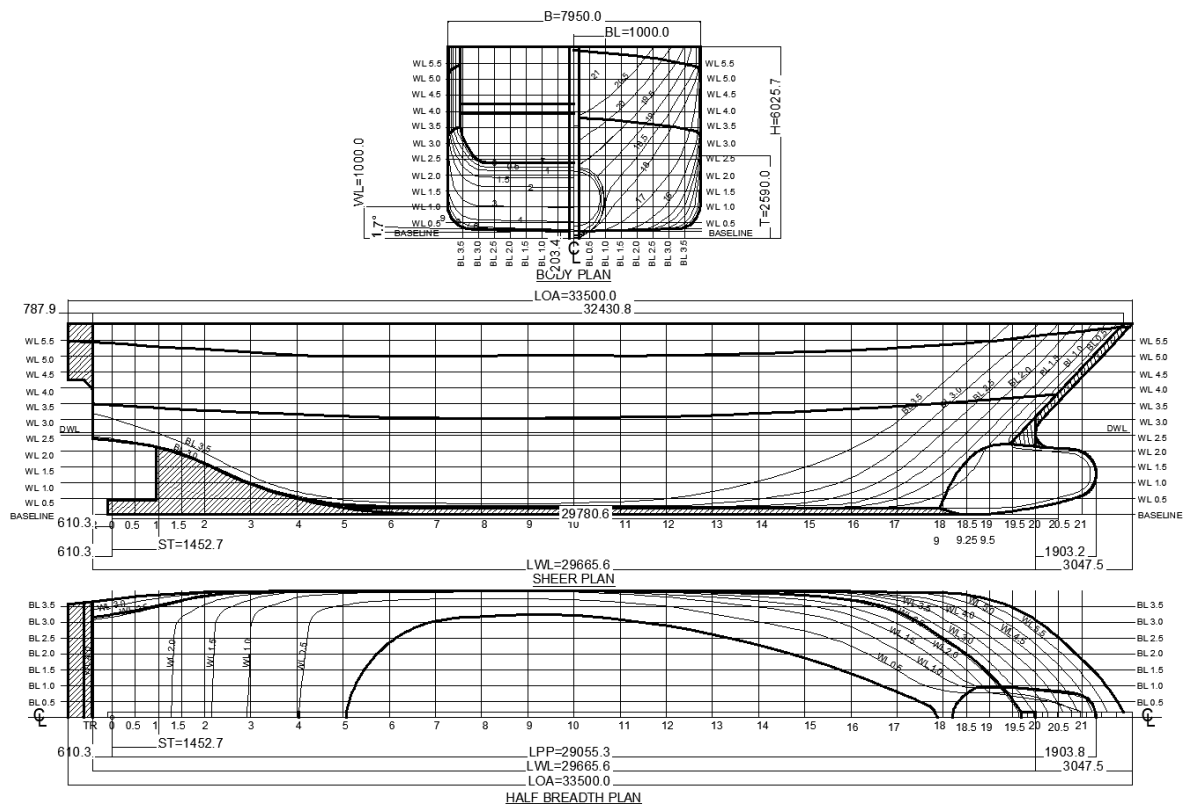


Figure 1. Golden Tuna Linesplan

TABLE 1.  
 PRINCIPAL DIMENSION

Parameter	Value	Unit
LOA	33.500	m
LPP	29.054	m
B	7.950	m
H	4.060	m
T	2.590	m
Displacement ( $\Delta$ )	415.6	ton
Gross Tonnage	265	ton

Based on the survey results, the vessel geometry was first reconstructed as a 2D linesplan to ensure consistency with the observed vessel characteristics. The lines plan, comprising the body plan, sheer plan, and half breadth plan, was subsequently verified for geometric fairness. The resulting Golden Tuna lines plan is presented in Figure 1. The principal dimensions of the surveyed tuna longliner represent the primary geometric characteristics of the vessel. The values were derived from field survey data and refined the principal dimension in Table 1. Presented in Figure 2, the general arrangement illustrates the spatial layout of

The main deck structures and the installation of the wingsail, the general arrangement provides an overview of the compartment distribution, deckhouse position, and working deck configuration, and serves as the basis for the assumed loading and weight distribution applied in the subsequent analysis, reconstructed from field survey observations of the reference vessel, which served as the mother ship for this study. Wingsail is positioned near the midship region, with the installation point adjusted to the available web frame location at approximately 17.4 m from the aft perpendicular (AP), to maintain

transverse balance and minimise adverse effects on the vessel's overall mass distribution.

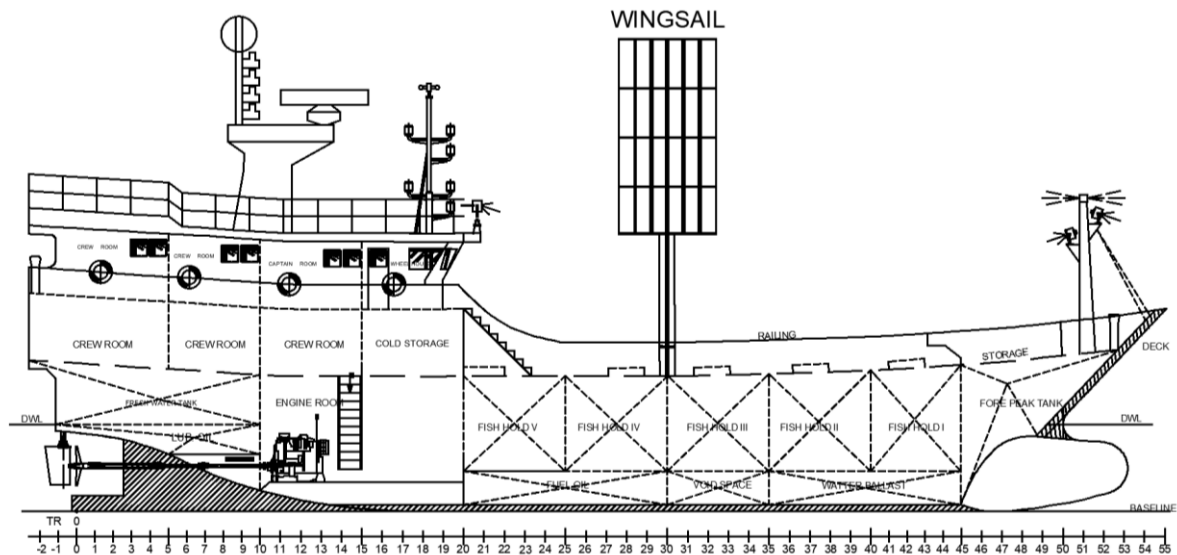


Figure 2. General Arrangement of a fishing vessel

b) Sail Configuration

Previous studies highlighted the effectiveness of rigid wingsails for wind-assisted propulsion and the importance of the installation layout in maintaining aerodynamic efficiency [6].

The structural design and material characteristics of wingsails also influence their feasibility and integration into vessel systems [12]–[15]. Among commonly used reference sections, the symmetric NACA 0015 airfoil is frequently used for rigid-wing sail studies due to its balanced aerodynamic performance [12].

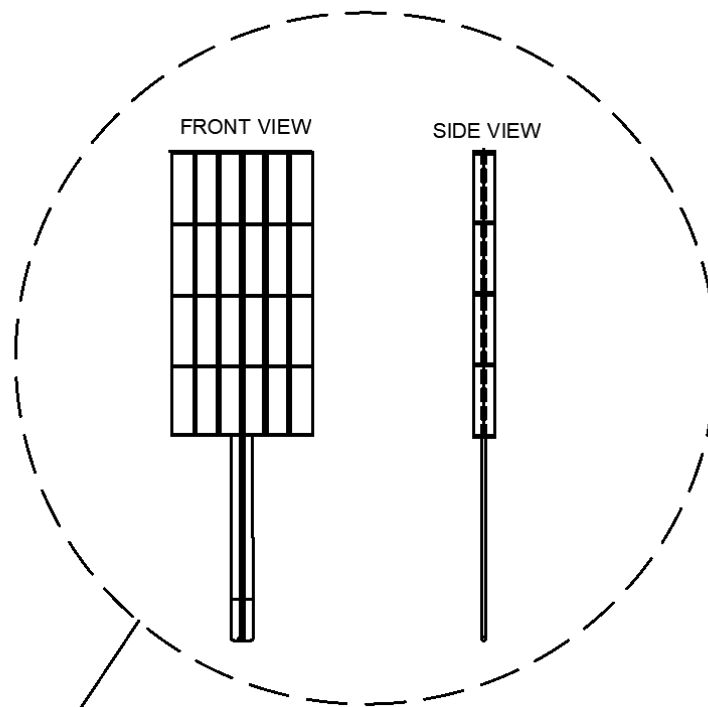


Figure 3. Wingsail Geometry

TABLE 2.  
 PRINCIPAL WINGSAIL DIMENSION

Parameter	Value	Unit
Chord (C)	2.85	m
Height (H)	10	m
Total Sail Area (A)	28.5	m <sup>2</sup>
Material	GFRP	-
Number Of Sail	1	-

Figure 3 presents the geometric configuration of the rigid wingsail adopted in this study. The principal dimensions of the wingsail are summarised in Table 2. The sail height was selected to ensure that the installation does not interfere with the forward visibility from the wheelhouse. In this configuration, the supporting mast height is approximately 4.2 m, thereby maintaining adequate visual clearance toward the bow. The wingsail mass was estimated using a component breakdown method based on material volume and GFRP density of  $\rho = 1800 \text{ kg/m}^3$ . The NACA 0015 airfoil profile has a section perimeter of 5.871 m, derived from 2.06 times the chord length [4]. The hollow structure comprises a 4 mm GFRP outer skin, five vertical spars of 3–6 mm thickness, four horizontal ribs of 4 mm thickness, and an aluminium rotation mast of  $\text{Ø}200 \times 10 \text{ mm}$ , with a 10% miscellaneous factor for bearings, fasteners, and coating [13]. The component breakdown yields a total estimated mass of 777.0 kg, dominated by the outer skin at 54.4% and the aluminium mast at 20.7%. The estimated mass was cross-checked against the mass-to-sail area ratio from existing wingsail systems. The Oceanbird Wing 560 has a ratio of approximately  $268 \text{ kg/m}^2$ , due to its high-strength steel construction for vessels exceeding 200 m [14]. The NASA Zephyr conceptual wingsail with a NACA 0015 profile yields a significantly lower ratio of  $4.1 \text{ kg/m}^2$  [5]. The present wingsail produces a ratio of  $27.3 \text{ kg/m}^2$ , which falls within the typical range of 20 – 30  $\text{kg/m}^2$  reported for composite marine wingsails [15]. Based on the component breakdown and scaling cross-check, the total wingsail mass, including the supporting structure and mounting system, was estimated at 1000 kg.

## B. Seakeeping and Stability Criteria

### a) Seakeeping

A vessel operating at sea experiences six degrees of freedom (6-DOF) motions, consisting of surge, sway, heave, roll, pitch, and yaw. The assessment focuses on the primary ship motions, namely heave, pitch, and roll, which represent the dominant dynamic responses of the fishing vessel under realistic operating conditions.

Vessel motion responses in waves are commonly evaluated using Response Amplitude Operators (RAO), which describe the relationship between wave excitation and ship motion [16], [17].

Response Amplitude Operator:

$$RAO = \frac{\zeta_{2\sigma}}{\zeta_0} \quad (1)$$

Wave Spectrum:

$$S(\omega) = \alpha g^2 / \omega^5 \cdot e^{-(5/4)(\omega_m/\omega)^4} \quad (2)$$

Encounter Wave:

$$\omega_e = \omega - kV \cos \mu \quad (3)$$

Heave response from vertical wave motion:

$$C_z = \frac{z}{h_w} \sqrt{RAO_z} \quad (4)$$

Roll response from lateral rotation:

$$C_\phi = \phi \frac{\sqrt{RAO_\phi}}{k} \quad (5)$$

Pitch response from longitudinal rotation:

$$C_\theta = \theta \frac{\sqrt{RAO_\theta}}{k} \quad (6)$$

The equations above describe the vessel's motion response characteristics in waves. Here,  $z$  is the heave displacement,  $h_w$  is the incident wave amplitude,  $\phi$  and  $\theta$  denotes the roll and pitch motions, respectively, and  $k$  is the wave number. The Response Amplitude Operator (RAO) is the ratio of the motion response amplitude to the wave amplitude. Furthermore,  $S(\omega)$  is the wave spectral density,  $\alpha$  is the Phillips constant,  $g$  is the gravitational acceleration,  $\omega$  is the wave circular frequency,  $\omega_m$  is the modal wave frequency,  $\omega_e$  is the encounter frequency,  $V$  is the ship speed, and  $\mu$  is the wave heading angle. These parameters collectively govern the prediction of vessel motions under sea state excitation.

TABLE 3.  
OPERATIONAL SEAWORTHINESS LIMIT CRITERIA

Criteria	NATO STANAG 4154	U.S. Coast Guard
Motion Sickness Incidence (MSI)	20% of the crew in 4 hours	5% in a 30-minute exposure
Motion Induced Interruption (MII)	1 tip per minute	2.1 tip per minute
Roll Amplitude	4.0 deg RMS	8.0 deg SSA
Pitch Amplitude	1.5 deg RMS	3.0 deg SSA

The operational seakeeping criteria presented in Table 3 serve as reference benchmarks for evaluating the acceptability of the vessel's motion responses. These limits guide the allowable levels of motion sickness incidence (MSI) and motion-induced interruptions (MII),

as well as roll and pitch amplitudes under operational conditions. In this study, the predicted motion responses are compared against these criteria to determine whether the vessel performance satisfies the recommended seakeeping requirements.

b) Stability Criteria

The intact stability assessment primarily considers the vessel's hydrostatic characteristics. The exposed windage areas of the superstructure and wingsail are defined in the model to represent the above-water geometry; however, the present study focuses on hydrostatic stability behaviour rather than a detailed wind-heeling evaluation. In this context, the transverse metacentric height (GM) is used to indicate the vessel's initial stability, while the righting arm (GZ) represents the restoring capability at finite heel angles. The static stability moment (M), obtained from the product of displacement and righting arm, reflects the overall effectiveness of the vessel's restoring performance. The transverse metacentric height (GM) is calculated based on the relationship between buoyancy and metacentre [19].

$$GM = KB + BM - KG \quad (7)$$

The static stability moment is given by the product of displacement and the righting lever.

$$M = W X GZ \quad (8)$$

Horizontal restoring lever during heel righting of the arm.

$$GZ = ls \cdot G \cdot \sin\theta = ls \cdot (Zg - Zgt) \cdot \sin\theta \quad (9)$$

The intact stability criteria listed in Table 4 are applied to evaluate the vessel's static stability performance in accordance with the IMO Code. These requirements specify the minimum acceptable limits for the righting arm characteristics and metacentric height to ensure sufficient restoring capability. In this study, the calculated stability parameters are compared with the prescribed limits to verify whether the vessel complies with the intact stability requirements under the considered loading condition.

TABLE 4.  
 INTACT STABILITY CRITERIA [20].

Criteria	Description
A	The area under the GZ curve from 0° to 30° heel shall not be less than 0.055 m·rad.
B	The area under the GZ curve from 0° to x (40°) heel shall not be less than 0.09 m·rad.
C	The area between 30° and x heel shall not be less than 0.03 m·rad, where x is 40° or less up to the angle at which water first enters the hull.
D	The maximum righting arm (GZ max) shall occur at a heel angle not less than 30°, with a minimum value of 0.20 m.
E	The maximum angle of positive stability shall be greater than 25°.
F	The metacentric height (GM) shall not be less than 0.15 m

C. Maxsurf setup

a) Maxsurf Modeler

The 3D hull geometry was developed using Maxsurf Modeller based on the reconstructed two-dimensional line plan. The modelling process ensured that the hull form remained fully consistent with the previously

verified geometric characteristics. Particular attention was given to surface fairness and dimensional fidelity to preserve the hydrostatic characteristics of the reference vessel. The superstructure arrangement and wing-sail placement were subsequently configured in accordance with the General Arrangement.

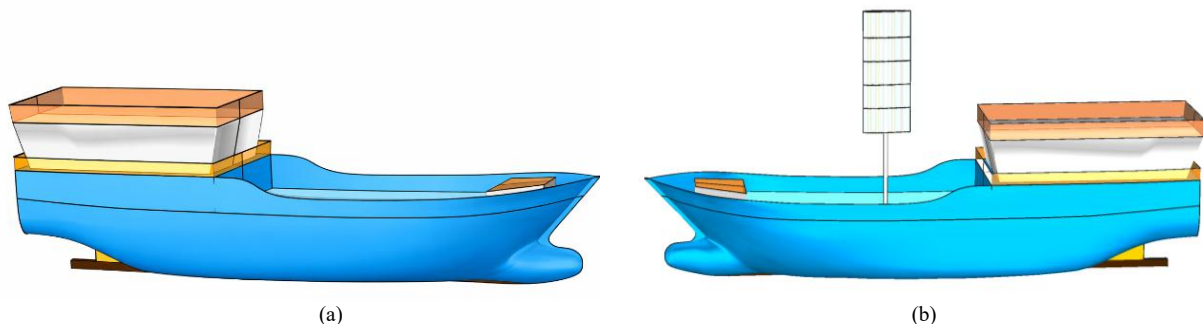


Figure 4. Three-dimensional geometric models of the vessel  
 (a) configuration without wingsail (b) modified configuration with wingsail.

Figure 4 (a) illustrates a three-dimensional model of the vessel without the wingsail installation, which serves as

the reference configuration. (b) presents the modified configuration in which the rigid wingsail system is

integrated into the vessel. Both configurations enable a consistent comparison framework while maintaining identical hull characteristics between cases.

b) Maxsurf Motion

The seakeeping analysis was performed on the fishing vessel with and without a wingsail to evaluate the seakeeping performance based on the operational seaworthiness limit criteria. The wingsail is mounted above the deck and does not alter the underwater hull geometry; its influence on seakeeping response is represented through changes in the vessel mass distribution properties. For the wingsail condition, the VCG was adjusted from 3.310 m to 3.324 m and the roll radius of gyration from 3.199 m to 3.208 m to account

for the wingsail mass distribution above deck. The empirical roll coefficient of 0.40 B was adopted following the validation with an  $r^2$  of 0.96. Displacement was maintained at 415.6 tons in both conditions, as the wingsail mass accounted for less than 0.2% of total displacement. Strip theory is applied to estimate the heave, roll, and pitch responses. The wave conditions in Table 5 were derived from wind and wave data observed in Benoa waters. The sea state height and wind speed classifications are referenced using the Beaufort Scale, which provides standardised limits for estimating sea states in offshore operations. The simulations were implemented in Maxsurf Motion using the ITTC two-parameter Pierson-Moskowitz spectrum. The software automatically set the peak enhancement factor to 1.0.

TABLE 5.  
 MOTION ANALYSIS OPERATIONAL PARAMETERS

Ship Speed (knots)	Wave Heading (deg)	Wind Direction (deg)	Sail Orientation (deg)	H <sub>1/3</sub> (m)	T <sub>p</sub> (s)
6	90	90	90	1.25	6
6	90	90	90	2.00	8
6	90	90	90	3.00	10
8	135	90	90	1.25	6
8	135	90	90	2.00	8
8	135	90	90	3.00	10
10	180	90	90	1.25	6
10	180	90	90	2.00	8
10	180	90	90	3.00	10

c) Maxsurf Stability

To evaluate the influence of wingsail installation on the vessel's stability characteristics, the analysis was performed for two configurations: the hull without wingsail and with wingsail. Each configuration was assessed under three representative operational load cases. Table 6 presents the departure loading condition, assuming the vessel leaves port with full operational consumables and the initial payload distribution. The weight

components are grouped to define the overall mass distribution and the corresponding vertical and longitudinal moments. Table 7 describes the intermediate operating condition at the fishing ground, where partial consumption of fuel, freshwater, and ballast is considered while the payload begins to increase. This load case reflects a realistic mid-voyage scenario of the fishing vessel. Table 8 represents the arrival loading condition of the vessel. In this scenario, the consumables such as fuel oil, fresh water, and lubricating oil are reduced following the operational voyage, while the fish hold is assumed to be fully loaded.

TABLE 6.  
 LOADCASE 1 DEPARTURE

Component	Weight (t)	KG(m)	Vertical Moment	LCG(m)	Longitudinal Moment
Lightship	260.000	3.314	861.640	14.527	3777.020
Fresh Water	15.284	2.782	42.520	2.152	32.891
Lubricating Oil	2.302	1.772	4.079	4.091	9.417
Fuel Oil	44.310	0.724	32.080	14.373	636.868
Water Ballast	12.808	0.520	6.660	22.703	290.780
Fish Hold	30.000	1.600	48.000	21.900	649.000
Crew (ABK)	10.000	3.000	30.000	10.000	100.000
Provision	8.000	2.500	20.000	10.000	80.000
TOTAL	382.704	2.73	1044.980	14.55	5568.976

TABLE 7.  
 LOADCASE 2 FISHING GROUND

Component	Weight (t)	KG(m)	Vertical Moment	LCG(m)	Longitudinal Moment
Lightship	260.000	3.314	861.640	14.527	3777.020
Fresh Water	10.421	2.722	28.366	2.162	22.530
LubricationOil	0.000	-	0.000	-	0.000
Fuel Oil	20.920	0.481	10.062	14.365	300.516
Water Ballast	0.000	-	0.000	-	0.000
Fish Hold	110.000	1.891	208.000	17.618	1512.000
Crew (ABK)	10.000	3.000	15.000	10.000	50.000
Provision	1.000	2.500	2.500	10.000	10.000
TOTAL	412.341	-	1157.568	-	5954.066

TABLE 8.  
 LOADCASE 3 ARRIVAL

Component	Weight (t)	KG(m)	Vertical Moment	LCG(m)	Longitudinal Moment
Lightship	260.000	3.314	861.640	14.527	3777.020
Fresh Water	12.505	2.748	34.364	2.158	26.980
Lubricating Oil	0.212	1.638	0.347	4.102	0.870
Fuel Oil	31.380	0.604	18.954	14.369	450.899
Water Ballast	6.564	0.384	2.521	22.655	148.707
Fish Hold	50.000	1.600	80.000	20.520	1020.000
Crew (ABK)	10.000	3.000	30.000	10.000	100.000
Provision	12.000	2.500	30.000	10.000	120.000
TOTAL	382.661	-	1057.825	-	5614.476

### III. RESULTS AND DISCUSSION

#### A. Seakeeping Performance

##### a) RAO Analysis

The RAO comparison between the wingsail and the configuration without wingsail is presented in Figure 5. The heave RAO at beam sea 90° peaks near unity at low frequencies around 0.4–0.6 rad/s, while at quarter sea 135° and head sea 180°, distinct resonance peaks emerge between 0.7–1.0 rad/s with maximum values reaching 1.3 and 1.4, respectively, at 10 knots. The roll RAO is most dominant at beam sea 90° with peak values of approximately 4.5–5.0 deg/m near the natural roll frequency around 1.0 rad/s, reducing to 2.0–3.0 deg/m at quarter sea 135° and effectively zero at head sea (180°). Due to symmetric wave loading. The pitch RAO shows the opposite trend, with the highest response occurring at head sea 180°, reaching 2.5–3.0 deg/m, followed by

quarter sea 135° and beam sea 90°, where longitudinal wave excitation is minimal. Across all headings, speeds, and degrees of freedom, the RAO curves for both configurations are nearly identical, indicating that the vessel’s motion response is predominantly governed by hull geometry and wave excitation rather than the presence of the wingsail. This behaviour can be attributed to the relatively small contribution of the wingsail mass to the total displacement, resulting in only minor changes in the vertical centre of gravity and the radius of gyration, which are insufficient to alter the vessel’s dynamic response significantly. This finding is consistent with [8], who reported that hard sail installation on a KVLCC2 tanker produced minimal change in motion amplitudes under head sea conditions. Similarly, [7] observed that above-deck structural additions primarily affect the roll RAO peak while pitch remains largely unchanged.

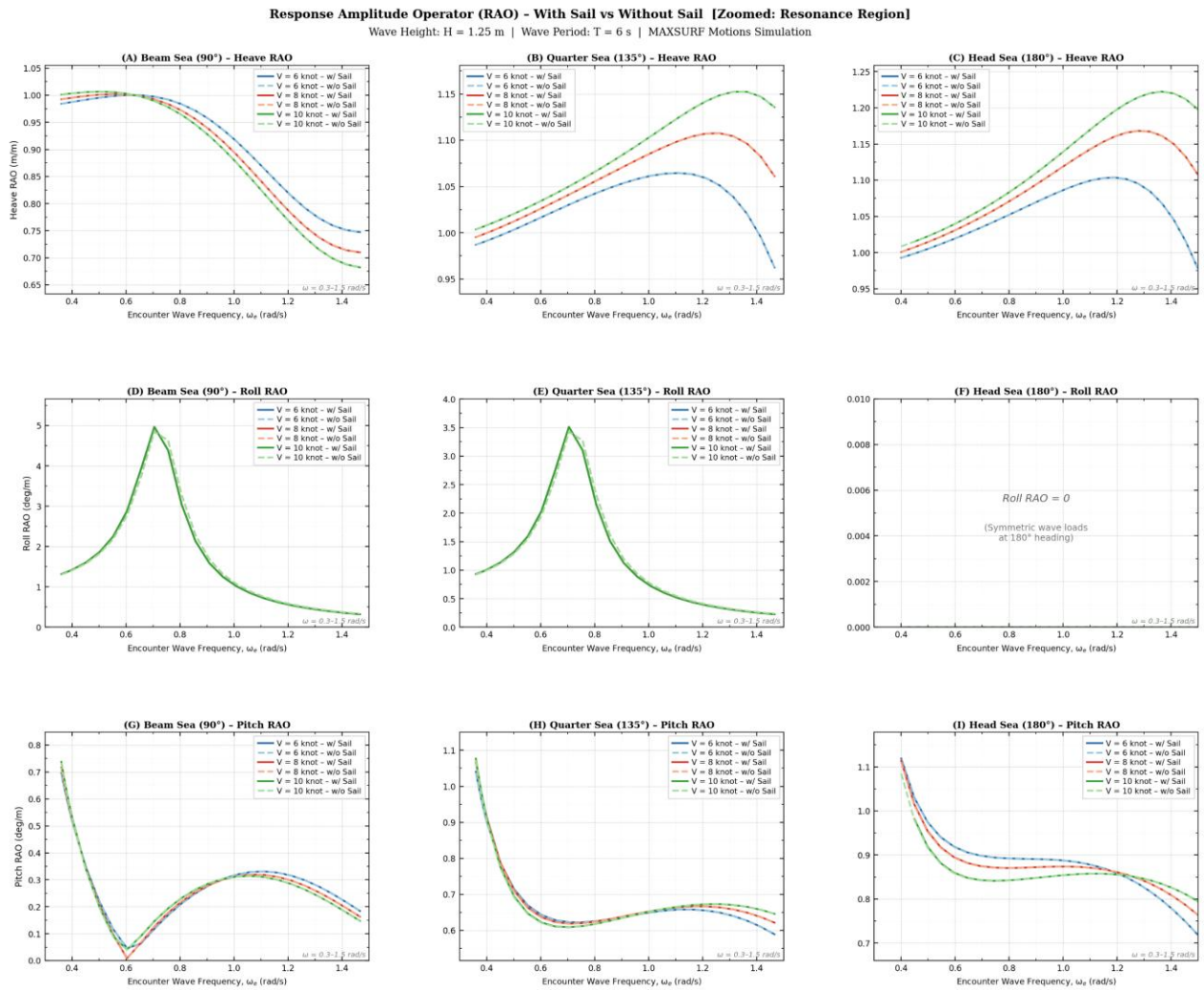


Figure 5. Comparison of RAO responses for the fishing vessel with and without a wingsail

b) RMS Response

TABLE 9.  
 RMS EVALUATION H=3M, T=10s

Speed	Heading	W/o sail (deg)	W/Sail (deg)	Roll Status (4.0°)	Pitch W/o sail (deg)	Pitch W/Sail (deg)	Pitch Status (1.5°)
10 kn	Head 180°	0.00	0.00	PASS	2.16	2.17	FAIL
10 kn	Quarter 135°	2.95	2.87	PASS	1.83	1.83	FAIL
10 kn	Beam 90°	6.72	6.60	FAIL	0.80	0.80	PASS
8 kn	Head 180°	0.00	0.00	PASS	2.24	2.24	FAIL
8 kn	Quarter 135°	3.24	3.16	PASS	1.85	1.85	FAIL
8 kn	Beam 90°	6.72	6.60	FAIL	0.81	0.81	PASS
6 kn	Head 180°	0.00	0.00	PASS	2.32	2.32	FAIL
6 kn	Quarter 135°	3.56	3.47	PASS	1.87	1.87	FAIL
6 kn	Beam 90°	6.72	6.60	FAIL	0.85	0.84	PASS

The RMS motion evaluation presented in Table 9 is conducted under the worst-case sea condition of H = 3 m and T = 10 s for Benoa operational waters. Roll motion remains within the 4.0° limit under head sea 180° and quarter sea 135°, while beam sea 90° produces the highest roll response at 6.72° without wingsail and 6.60° with wingsail, both exceeding the criterion. Pitch motion under head sea ranges from 2.16° to 2.32°, exceeding the

1.5° limit, whereas beam sea remains within acceptable limits. The comparison between configurations shows only minor differences. That suggests that the wingsail installation has a negligible effect on motion amplitudes, and that the observed responses are primarily controlled by wave-hull interaction rather than by topside modifications. The identical exceedances observed in both configurations indicate that these limitations

originate from inherent hull-form characteristics, highlighting that improvements in seakeeping performance should focus on hull design optimisation rather than on auxiliary system modification [9]. Similar findings were reported in [8], where hard sail installation did not produce a significant change in motion amplitudes.

The MSI evaluation presented in Table 10 is conducted under the same worst-case sea condition of  $H = 3$  m and  $T = 10$  s. The results indicate that vertical acceleration values at all speeds and headings remain below the 20% MSI threshold, which ranges from 0.731 to 0.878  $m/s^2$ . The highest acceleration occurs under head sea  $180^\circ$  at 10 knots, reaching 0.688  $m/s^2$ , while the lowest value is observed under beam sea conditions. All calculated values are below the MSI limit, so both configurations meet the comfort criteria. The wingsail does not significantly influence vertical acceleration and remains within acceptable limits under these conditions.

c) MSI and MII Evaluation

TABLE 10.  
MSI EVALUATION H=3M, T=10s

Speed	Heading	W/Sail ( $m/s^2$ )	Wo/Sail ( $m/s^2$ )	20% MSI ( $m/s^2$ )	Status
10 kn	Head $180^\circ$	0.688	0.688	0.878	PASS
10 kn	Quarter $135^\circ$	0.635	0.635	0.862	PASS
10 kn	Beam $90^\circ$	0.339	0.339	0.743	PASS
8 kn	Head $180^\circ$	0.582	0.582	0.841	PASS
8 kn	Quarter $135^\circ$	0.559	0.559	0.827	PASS
8 kn	Beam $90^\circ$	0.355	0.355	0.731	PASS
6 kn	Head $180^\circ$	0.481	0.481	0.806	PASS
6 kn	Quarter $135^\circ$	0.488	0.426	0.737	PASS
6 kn	Beam $90^\circ$	0.375	0.375	0.731	PASS

TABLE 11.  
MII EVALUATION H=3M, T=10s

Speed	Heading	W/o Sail	W/Sail (MII/h)	Limit	Status
10 kn	Head $180^\circ$	0.000	0.000	1 tip/min	PASS
10 kn	Quarter $135^\circ$	0.017	0.014	1 tip/min	PASS
10 kn	Beam $90^\circ$	3.131	2.969	1 tip/min	PASS
8 kn	Head $180^\circ$	0.000	0.000	1 tip/min	PASS
8 kn	Quarter $135^\circ$	0.035	0.029	1 tip/min	PASS
8 kn	Beam $90^\circ$	3.136	2.975	1 tip/min	PASS
6 kn	Head $180^\circ$	0.000	0.000	1 tip/min	PASS
6 kn	Quarter $135^\circ$	0.074	0.062	1 tip/min	PASS
6 kn	Beam $90^\circ$	3.143	2.982	1 tip/min	PASS

The MII evaluation presented in Table 11 shows that tipping values for both configurations remain well below the NATO STANAG 4154 limit of 1 tip per minute across all headings and speeds. The highest MII was recorded at beam sea  $90^\circ$  with 3.143 MII/h without wingsail and 2.969 MII/h with wingsail, equivalent to approximately 0.052 tip per minute, significantly below the allowable threshold. At head sea  $180^\circ$ , the MII is effectively zero for both conditions, while quarter sea  $135^\circ$  produces negligible values ranging from 0.014 to 0.074 MII/h. The slightly lower MII values in the wingsail configuration can be associated with the increased roll radius of gyration, which enhances rotational inertia and contributes to a minor reduction in roll-induced interruptions. However, the effect remains limited in magnitude. Despite the RMS exceedances at

beam sea and head sea, both MSI and MII remain within acceptable limits across all nine operating conditions, confirming that overall crew comfort and operational safety are not critically compromised [17]. This finding shows that MSI and MII more fully assess operational performance by reflecting crew comfort and operability under realistic sea conditions.

**B. Stability Criteria**

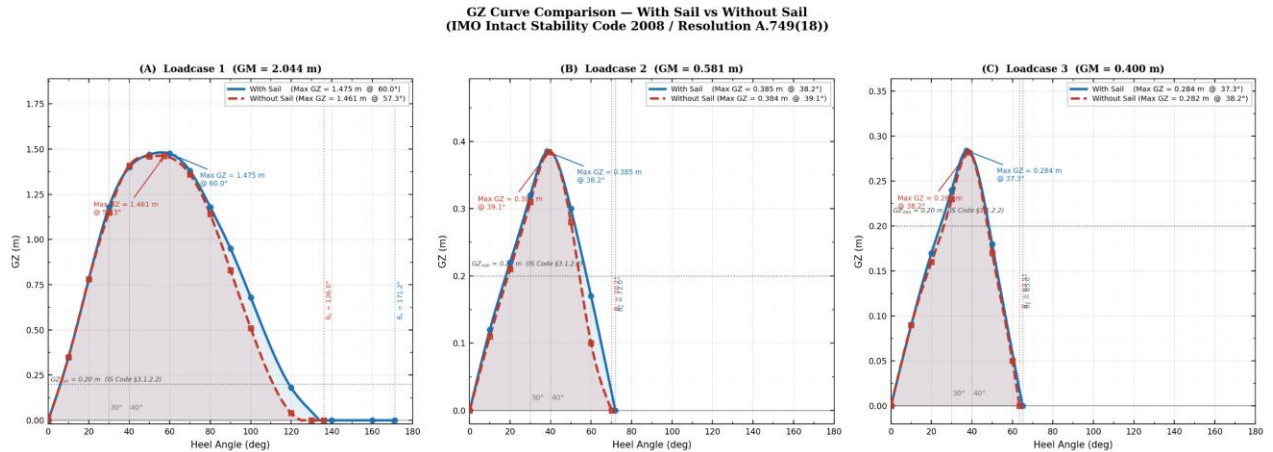


**Figure 6.** GZ Curve Comparison With and Without Sail

**TABLE 12.**  
INTACT STABILITY CRITERIA COMPLIANCE INTACT STABILITY CRITERIA COMPLIANCE [20]

Criteria	Requirement	W/Sail LC1	W/Sail LC2	W/ Sail LC3	W/o Sail LC1	W/o Sail LC2	W/o Sail LC3	Status
A	Area 0°–30° ≥ 0.055 m·rad	0.3003	0.0875	0.0665	0.2975	0.0829	0.0638	Pass
B	Area 0°–40° ≥ 0.090 m·rad	0.5283	0.1510	0.1138	0.5236	0.1453	0.1101	Pass
C	Area 30°–40° ≥ 0.030 m·rad	0.2280	0.0634	0.0472	0.2261	0.0623	0.0463	Pass
D	GZ max ≥ 0.20 m at angle ≥ 30°	1.475 m at 60°	0.385 m at 38.2°	0.284 m at 37.3°	1.461 m at 57.3°	0.384 m at 39.1°	0.282 m at 38.2°	Pass
E	Angle of GZ max > 25°	60.0°	38.2°	37.3°	57.3°	39.1°	38.2°	Pass
F	GM ≥ 0.15 m	2.044 m	0.581 m	0.400 m	2.044 m	0.581 m	0.400 m	Pass

Figure 6 presents the GZ curves for all three load cases under both with-sail and without-sail conditions, where Loadcase 1 yields the highest righting arm GZ max 1.475 m with sail, 1.461 m without sail, while Loadcase 3 produces the lowest 0.284 m and 0.282 m, respectively. Table 12 confirms that all six conditions satisfy the six intact stability criteria of IMO IS Code 2008. For the with sail condition, the most critical margin is found in Loadcase 3 Criterion A, where the computed area of 0.0665 m·rad exceeds the minimum requirement of 0.055 m·rad by 21%, while for the without sail condition the same criterion yields a narrower margin of 16% with a value of 0.0638 m·rad, indicating that the absence of sail results in a slightly more critical stability condition in the lower heel angle region. Overall, the wingsail configuration demonstrates a marginal improvement in righting characteristics. Properly distributed extra mass above deck does not degrade hydrostatic stability and may even improve restoring performance under certain loading conditions.

**IV. CONCLUSION**

This study evaluates the effects of rigid wingsail integration on seakeeping and intact stability of a 33.5 m tuna longliner. The results show that adding a wingsail does not significantly affect vessel motion. Seakeeping remains similar with or without the wingsail. All loading conditions meet the IMO Intact Stability Code 2008 criteria, showing only marginal differences between the two setups.

Some motion limits are exceeded under specific wave headings in both setups. That is likely due to inherent hull features, not the wingsail. Thus, wingsail integration is technically feasible and does not compromise safety or performance.

**V. ACKNOWLEDGEMENTS**

The authors gratefully acknowledge the Hydrodynamics Technology Research Center, National Research and Innovation Agency (BRIN), Surabaya, Indonesia, for providing vessel data, simulation facilities, and technical support throughout this research. The authors also acknowledge the Department of Marine Engineering, Universitas Pembangunan Nasional Veteran Jakarta, Indonesia, for academic support during the completion of this study.

**REFERENCES**

- [1] V. R. Kurniawati, R. W. Birmingham, A. J. Murphy, D. P. Yuwandana, P. I. Wahyuningrum, E. S. Wiyono, Y. Novita, and B. H. Iskandar, "Energy consumption of traditional fishing vessels in Palabuhanratu, Indonesia," *AACL Bioflux*, vol. 16, no. 2, pp. 929–944, 2023.
- [2] M. Kolodziejcki and M. Sosnowski, "Review of wind-assisted propulsion systems in maritime transport," *Energies*, vol. 18, no. 4, p. 897, 2025, doi: 10.3390/en18040897.
- [3] N. Deeb, A. Baidowi, and A. Kurniawan, "Flettner rotor modification through adding ridges and fins with results comparison to base model," *Int. J. Mar. Eng. Innov. Res.*, vol. 8, no. 2, 2023.
- [4] N. I. B. Ariffin and M. A. Hannan, "Wingsail technology as a sustainable alternative to fossil fuel," *IOP Conf. Ser.*:

- Mater. Sci. Eng., vol. 788, no. 1, p. 012062, 2020, doi: 10.1088/1757-899X/788/1/012062.
- [5] M. F. Silva, A. Friebe, B. Malheiro, P. Guedes, P. Ferreira, and M. Waller, "Rigid wing sailboats: A state of the art survey," *Ocean Engineering*, vol. 187, p. 106150, 2019, doi: 10.1016/j.oceaneng.2019.106150.
- [6] S. van Reen, J. Lin, J. Niu, P. Sharpe, X. Li, and H. D. Yao, "Reducing aerodynamic interference through layout optimisation of symmetrically cambered wingsails," *J. Mar. Sci. Eng.*, vol. 13, no. 10, p. 1998, 2025, doi: 10.3390/jmse13101998.
- [7] N. T. H. Trang, T. Mitsuyuki, Y. Hirakawa, K. Sadakata, and Y. Nakamura, "Experimental and numerical study on the seakeeping performance of a wind-powered generation ship," *J. Mar. Sci. Eng.*, vol. 13, no. 3, p. 412, 2025, doi: 10.3390/jmse13030412.
- [8] J. I. Chowdhury, A. Faieq, and O. M. Amin, "Seakeeping analysis of a tanker with hard sail-based wind propulsion system in various seaways," *Ocean Engineering*, vol. 289, p. 116252, 2023, doi: 10.1016/j.oceaneng.2023.116252.
- [9] N. J. D. D. Gómez Rojas, "Design criteria for seakeeping and stability of fishing vessels in regular waves," M.S. thesis, Chalmers Univ. Technol., Gothenburg, Sweden, 2021.
- [10] M. Iqbal, M. Terziev, T. Tezdogan, and A. Incecik, "Improving seakeeping performance of fishing boats by minimising radius of gyration," in *Proc. Global Maritime Congress, Istanbul, Türkiye, 2024*.
- [11] D. Purnamasari, M. R. Utina, Rina, E. Suwarni, and N. Setiyobudi, "Model experiment on fishing vessel operation in Benoa, Bali, using wind-assisted propulsion system," *Research Rep.*, BRIN, Surabaya, Indonesia, 2025.
- [12] H. Zhu, H. Yao, F. Thies, et al., "Propulsive performance of a rigid wingsail with crescent-shaped profiles," *Ocean Eng.*, vol. 285, p. 115349, 2023, doi: 10.1016/j.oceaneng.2023.115349.
- [13] F. Rubino, A. Nisticò, F. Tucci, and P. Carlone, "Marine application of fiber reinforced composites: A review," *J. Mar. Sci. Eng.*, vol. 8, no. 1, p. 26, 2020, doi: 10.3390/jmse8010026.
- [14] AlfaWall Oceanbird, "Oceanbird Wing 560 – product specifications," 2024. [Online]. Available: <https://www.theoceanbird.com/oceanbird-wing-560/>
- [15] R. Grin, "On empirical methods to predict the rolling period of ships," in *Proc. 15th Int. Marine Design Conf. (IMDC), Amsterdam, Netherlands, 2024*.
- [16] W. J. Pierson and L. Moskowitz, "A proposed spectral form for fully developed wind seas," *J. Geophys. Res.*, vol. 69, no. 24, pp. 5181–5190, 1964, doi: 10.1029/JZ069i024p05181.
- [17] A. Dinsbacher, "Evaluation of ship motion responses in waves using response amplitude operators (RAOs)," M.S. thesis, Hamburg Univ. Technol., Hamburg, Germany, 2010.
- [18] S. Ghaemi and P. Olszewski, "Analysis of seakeeping criteria for high-speed vessels based on motion sickness and operability indices," *J. Mar. Sci. Appl.*, vol. 16, no. 1, pp. 24–32, 2017, doi: 10.1007/s11804-017-1405-5.
- [19] A. Biran and R. López-Pulido, *Ship Hydrostatics and Stability*, 3rd ed. Oxford, U.K.: Butterworth-Heinemann, 2024.
- [20] International Maritime Organization (IMO), *International Code on Intact Stability, 2008 (2008 IS Code), Resolution MSC.267(85)*, 2008. [Online]. Available: [https://www.wcdn.imo.org/localresources/en/KnowledgeCentre/IndexofIMOResolutions/MSCResolutions/MSC.267\(85\).pdf](https://www.wcdn.imo.org/localresources/en/KnowledgeCentre/IndexofIMOResolutions/MSCResolutions/MSC.267(85).pdf)